The 2014 International Power Electronics Conference

Harmonic Modeling of a Vehicle Traction Circuit Towards the DC Bus

Saeid Haghbin, Andreas Karvonen and Torbjörn Thiringer
Division of Electric Power Engineering, Chalmers University of Technology, Gothenburg, Sweden
E-mails: saeid.haghbin@chalmers.se, andreas.karvonen@chalmers.se, torbjorn.thiringer@chalmers.se

***Abstract*—Different converters such as the traction inverter and DC/DC converter are connected to the dc bus of an electric or hybrid electric vehicle. Harmonic models of these devices towards the dc bus are needed to investigate different phenomena like the dc bus transients and ripples. A high-frequency harmonic model of a traction circuit, a drive system based on a three-phase inverter connected to an ac motor, is presented and explained. The model is extracted from an analytical approach developed for a three-phase inverter with a sinusoidal PWM controller. In addition to the analytical formulation, simulations and experimental results of a plug-in vehicle are provided to verify the spectrum of the dc bus waveforms.**

***Index Terms*—DC bus quality, frequency spectrum, harmonic model, three-phase inverter, vehicle traction.**

I. Introduction

The concept of more electric vehicle contrives more investigations at different system and component levels within the electrical system of a modern vehicle. Increasing the share of electrical components like the traction circuit or auxiliary systems brings more issues to be considered like component sizing, dc bus system quality, and harmonics. Normally, the vehicle powertrain is the heaviest load in the system; it can be around 50 kW for a typical passenger car. Hence, the impact of traction circuit on the vehicle dc bus is considerable which needs attention.

Several devices are connected to the system dc bus [1] like DC/DC converters, the battery, the battery charger [2], and the traction inverter within the vehicle electrical system. High frequency switching is usually an inherent feature of a controlled modern power electronic device. High frequency components in the voltages and currents are inevitable in the different parts of the system which is considered as an adverse impact. For example, the harmonic currents at the dc bus can result in a considerable amount of voltage ripple that can affect sensitive communication devices. Another disadvantage is the possible battery life reduction due to harmonics in the current. Hence, it is desirable to have a high frequency model in which the complexity and accuracy of the model can be adjusted by considering the phenomena of interest [3]–[6]. In this paper, a high frequency model of traction system towards the dc bus is utilized to investigate the dc bus harmonics.

Fig. 1 shows a simple diagram of traction circuit of a vehicle which is based on a three-phase inverter and an ac motor. In this scheme, the battery is connected to the inverter through a cable that can be of a significant length. Here, it is supposed that the battery is directly connected to the inverter and there is no DC/DC converter in the path. The battery and the cable are modeled as an ideal voltage source in series with an RL circuit. For a cable with the length of 5-10 m, this model is accurate enough [7] to investigate the dc bus harmonics in a frequency range of dc up to 100 kHz.

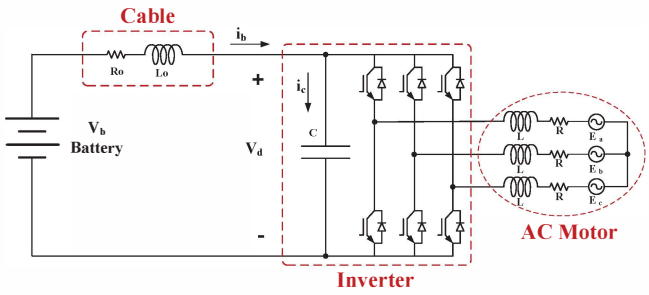

Fig. 1: Vehicle traction system based on a three-phase inverter.

The traction system from the dc terminal is usually modeled as a current source with a constant power [8] in which there is no information of the frequency components of the current and voltage. A high frequency model of a three-phase inverter with an ideal sinusoidal currents at the ac side is developed in [9] which is described at the following. The developed harmonic model is applied to a drive system with the rotor field-oriented control (FOC) and sinusoidal pulse width modulation (SPWM).

The main aim of this work is to provide a high-frequency equivalent circuit that can be used to investigate the dc bus voltage quality, for instance its frequency spectrum, for a FOC-based drive system. Simulation results are provided to investigate the dc bus voltage harmonics during steady state operation of the traction system. The battery current is also considered in the presented model. Some practical measurements of a commercial plug-in vehicle are presented.

After this introduction, the FOC scheme of the traction system is shortly presented. The high frequency model of the inverter system towards the dc bus is explained in section III. Simulation and practical measurements are presented in section IV and finally some conclusions are provided in the last section.

II. Field-Oriented Control of a PM Motor

FOC in the rotor reference frame (dq) is one of the widely used control schemes for traction applications which is shortly

978-1-4799-2705-0/14/$31.00 ©2014 IEEE

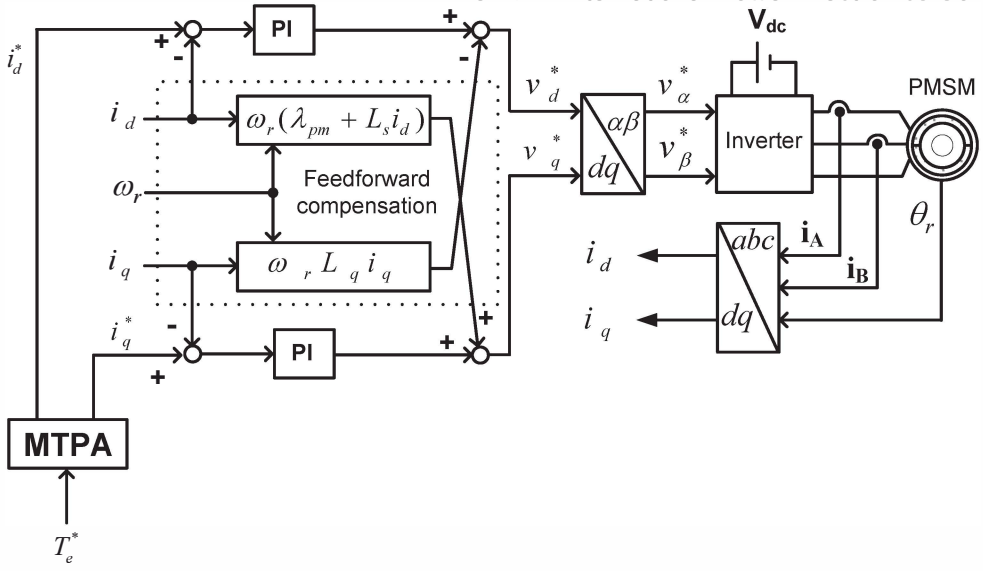

Fig. 2: Field-oriented control of a three-phase ac motor for the vehicle traction.

presented here. The following equations describe the mathematical model of a PM motor in the rotor reference frame:

$$v_d = r_s i_d + L_d \frac{d}{dt} i_d - \omega_r L_q i_q \tag{1}$$

$$v_q = r_s i_q + L_q \frac{d}{dt} i_q + \omega_r (\lambda_{PM} + L_d i_d) \tag{2}$$

where v_d, v_q, i_d and i_q are the voltages and currents in d and q axes respectively. Moreover, r_s, L_d, L_q, λ_{PM}, and ω_r are the stator resistance, the dq stator inductances, the permanent magnet flux linkage and the rotor electrical speed, respectively. The developed electromechanical torque can be written as

$$T_e = \frac{P}{2}\frac{3}{2}\{\lambda_{PM} i_q + (L_d - L_q) i_d \, i_q\} \tag{3}$$

where T_e is the torque and P is the number of poles.

A. Structure of the FOC for the IPM

Fig. 2 shows a schematic diagram of the drive structure [10], [11]. The system is a torque controller which is typical in traction applications. As can be seen in the figure, the reference torque is mapped to reference dq currents which form inputs to the high-bandwidth current controllers. A maximum torque per ampere (MTPA) strategy is typically used for this mapping [12] which can be a simple mapping table or a more accurate model [13].

Two independent PI controllers regulate the dq currents. The controller outputs are dq voltages that are compensated by feedforward terms to enhance the system response. The generated voltages are reference signals for the inverter which are transformed to the abc domain by using the Park and Clarke inverse transformation. Then the inverter produces the voltages by using the SPWM scheme. In steady state, the motor currents constitute symmetrical three-phase waveform with a fundamental frequency and some high frequency components. Consequently, the analytical model explained in the next section is developed for a system with three-phase currents.

B. The DC Bus Model

For the harmonic analysis, rather than an ideal voltage source, a frequency dependent model of the dc source is needed. The battery has an internal impedance that can be a complicated function of the frequency, temperature, current level and state of charge [14]. In this paper a simple RL circuit model is utilized to connect the battery to the inverter. This equivalent circuit includes the cable and battery as shown in Fig. 1. The equations describing the equivalent circuits are

$$i_c = C \frac{dv_d}{dt} \tag{4}$$

$$V_b = R_o i_b + L_o \frac{di_b}{dt} + V_d \tag{5}$$

where L_o, R_o, C, V_b and V_d are the cable and source inductance, the cable and source resistance, the inverter capacitance, the battery open circuit voltage and the inverter voltage at the point of connection, respectively.

III. Harmonic Model of a Three-Phase Inverter Towards the DC Bus

The dc bus capacitor filters the highly distorted inverter dc side current to provide a smoother current waveform from/to the dc source, a battery for instance. This capacitor is a bulky device that should be kept to a minimum size. However, the quality of the dc waveforms depends on its capacitance. A harmonic analysis in time-frequency domain is presented in

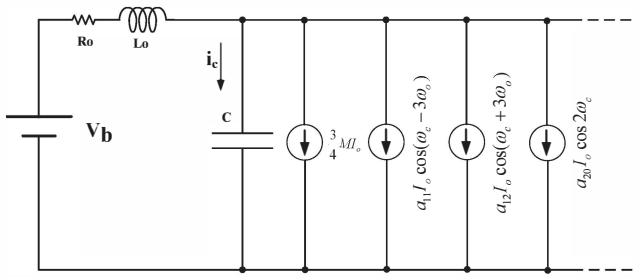

Fig. 3: Proposed high-frequency model of the inverter and load for frequency analysis.

[9] which provides a high-frequency equivalent circuit of a three-phase SPWM inverter towards the dc terminals.

The inverter dc side current, i_{inv}, can be written as [15]

$$i_{inv} = S_A\ i_A + S_B\ i_B + S_C\ i_C \tag{6}$$

where i_A, i_B and i_C are inverter currents at the ac side and S_A, S_B, and S_C are switches status, either 1 or 0.

Assume that the inverter is connected to a symmetrical three-phase load with pure sinusoidal waveform with a power factor of $cos\phi$. The inverter line currents can be described as

$$i_A = I_o\ cos(\omega_o t + \phi) \tag{7}$$

$$i_B = I_o\ cos(\omega_o t - \frac{2\pi}{3} + \phi) \tag{8}$$

$$i_C = I_o\ cos(\omega_o t + \frac{2\pi}{3} + \phi) \tag{9}$$

where I_o is the magnitude of the current, and ω_o is the angular frequency.

For an inverter with a SPWM control strategy the inverter dc side current, i_{inv}, is [9]

$$\begin{aligned} i_b = {} & \frac{3}{4}MI_o cos\phi + I_o\frac{3}{\pi}\{ \\ & ... + \sqrt{J_2^2(\frac{\pi}{2}M) + J_4^2(\frac{\pi}{2}M) - 2J_2(\frac{\pi}{2}M)J_4(\frac{\pi}{2}M)\ cos(2\phi)} \\ & cos(\omega_c t - 3\omega_o t + \phi_{11}) \\ & + \sqrt{J_2^2(\frac{\pi}{2}M) + J_4^2(\frac{\pi}{2}M) - 2J_2(\frac{\pi}{2}M)J_4(\frac{\pi}{2}M)\ cos(2\phi)} \\ & cos(\omega_c t + 3\omega_o t + \phi_{12}) + ... \\ & ... - \frac{2}{2}J_1(2\frac{\pi}{2}M)\ cos(\phi)\ cos(2\omega_c t) + ... \\ & \}. \end{aligned} \tag{10}$$

where $J_\alpha(x)$ is the Bessel function of the first kind, and M is the modulation index.

A simple model of the inverter is to replace the unit by a constant current source. This model can not be used to explain the high frequency ripple on the dc bus. Based on the developed equations of the inverter system at the dc side, as is presented in (10), a more accurate equivalent circuit can be used. Fig. 3 shows the proposed equivalent circuit where coefficients a_{11}, a_{12} and a_{20} are defined by (10).

The dc source and cable are modeled as an ideal voltage source and an RL impedance; a more accurate model can be utilized depend on the type of application. Moreover, the dc component of the load and high frequency components due to PWM switching are modeled as a summation of current sources. The number of high frequency current sources can be increased if a more accurate model is needed.

The above model includes important frequency information of the system. For example, the resonance frequency of the system due to the interaction of the dc cable that has an inductance value of L_o with the filter capacitor C is

$$f_r = \frac{1}{2\pi}\frac{1}{\sqrt{L_o C}} \tag{11}$$

where f_r is the resonance frequency. Moreover, the main harmonic components in the system are around multiples of carrier frequencies, i.e. $\omega_c t \pm 3\omega_o t$ and $2\omega_c t$. As is shown in [9] and can be seen later on in the simulations, the higher-order harmonics can be neglected.

IV. Simulation Results and Practical Verification

A. Simulation Results

For a commercial plug in vehicle the traction system is simulated with a dc bus voltage of $343\ V$. To evaluate the drive system performance, software simulations have been performed for a $20\ kW$ system in Matlab/Simulink; ideal switches are assumed for the inverter. Moreover, the dc bus capacitor is ideal (no ESL or ESR) and an RL network is assumed for the battery internal impedance and the cable connecting to the inverter. The parameters of the electric motor used for the simulation are presented in Table I.

TABLE I: Electric motor parameters.

	Value	Unit
Rated power	20	kW
Rated speed	3000	r/min
No of poles	10	-
Permanent magnet flux (λ_{PM})	0.0497	Wb
Stator resistance	0.0117	Ohm
d-axis inductance (L_d)	236	μH
q-axis inductance (L_q)	395	μH

The PWM frequency is $10\ kHz$ and the parameters of the dq controllers are selected according to [11]. For the motor, the values of L_d , L_q and λ_{PM} are considered constant during the simulations. For the harmonic analysis, with a frequency range of $0 - 100\ kHz$, it is not expected to have a perfect match between the simulations and measurement because of lack of accurate models and parameters. However, one can study the nature of different phenomena. For example, it is very easy to see how the cable inductance affects the dc bus voltage ripple.

Fig. 4 and Fig. 5 show the motor torque and speed for the simulation case. The speed is almost constant but there are slight ripples on the torque which is typical in such applications. The reference values of the dq currents are set to $i_d^\star = -105\ A$ and $i_q^\star = 162\ A$. The developed torque is around $81\ Nm$ and the motor speed is $2262\ rpm$; here a load proportional to the speed is assumed.

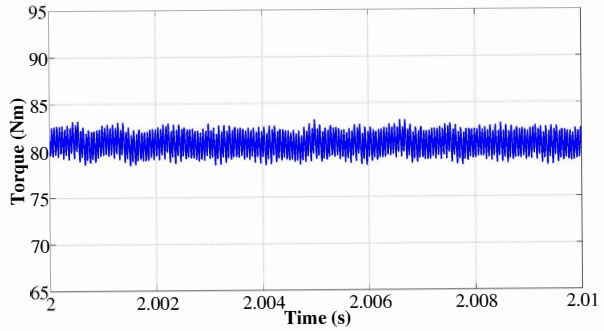

Fig. 4: Simulation: electromagnetic torque of the motor.

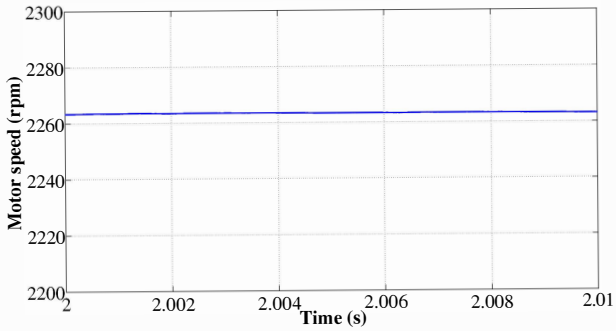

Fig. 5: Simulation: speed of the motor.

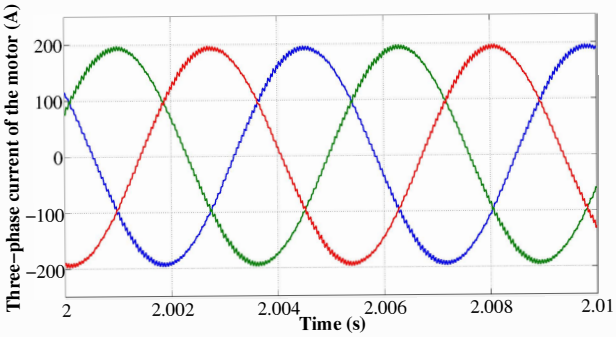

Fig. 6: Simulation: the motor three-phase currents at 2262 rpm and 81 Nm.

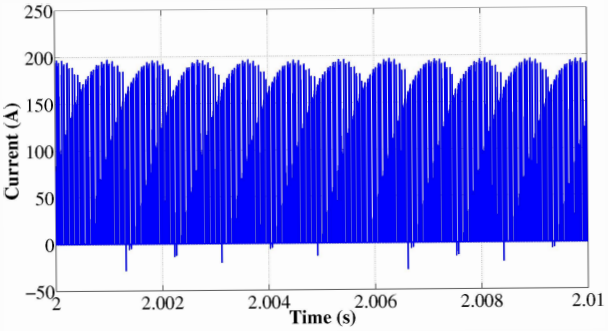

Fig. 7: Simulation: inverter dc side current at 2262 rpm and 81 Nm.

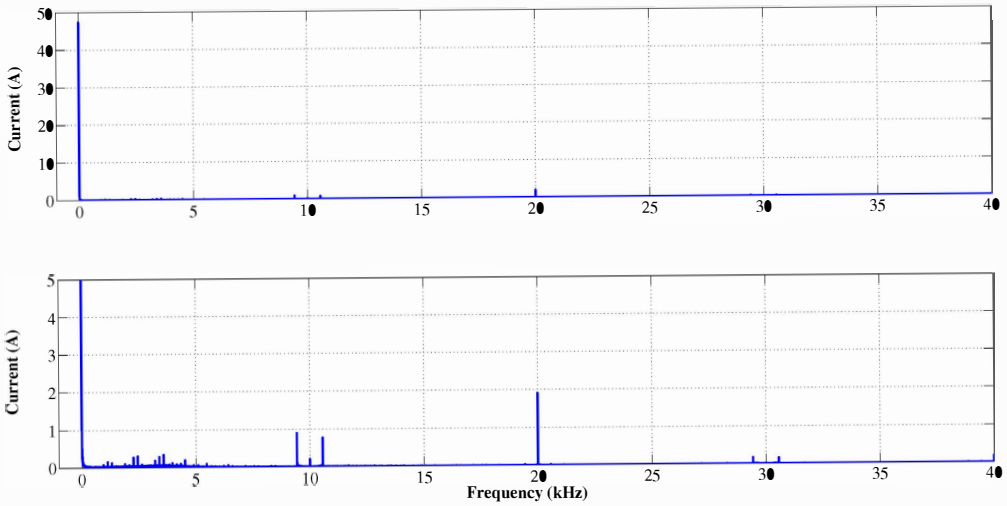

Fig. 8: Simulation: frequency spectrum of the battery current at 2262 rpm and 81 Nm: full spectrum (top) and a zoomed plot (bottom).

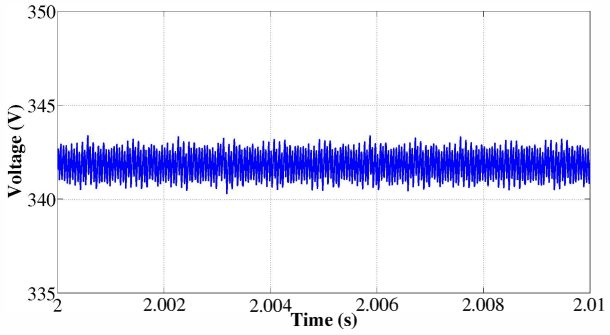

Fig. 9: Simulation: dc bus voltage over the main capacitor at 2262 rpm and 81 Nm.

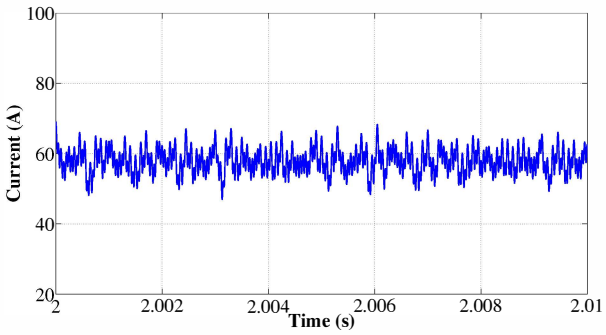

Fig. 10: Simulation: battery current at 2262 rpm and 81 Nm.

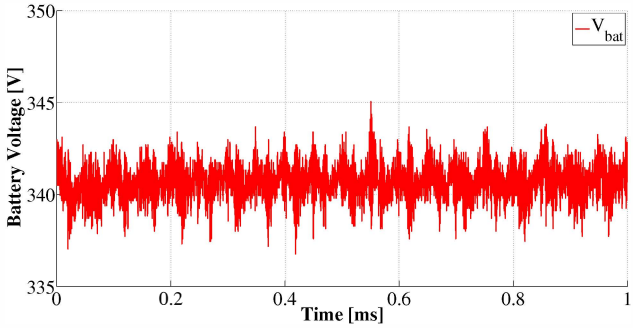

Fig. 11: Measurement: Battery voltage at 2262 rpm and 81 Nm.

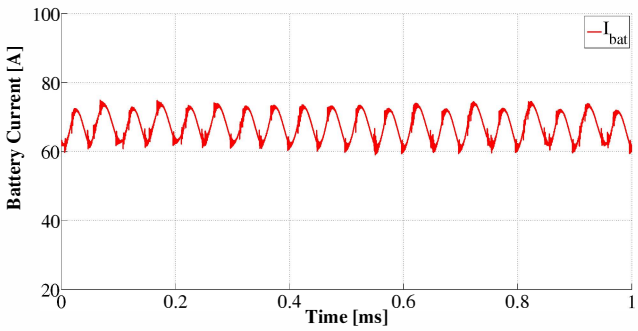

Fig. 12: Measurement: Battery current at 2262 rpm and 81 Nm.

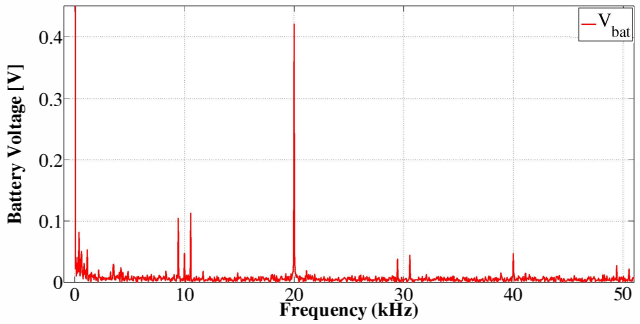

Fig. 13: Measurement: frequency spectrum of the battery voltage at 2262 rpm and 81 Nm.

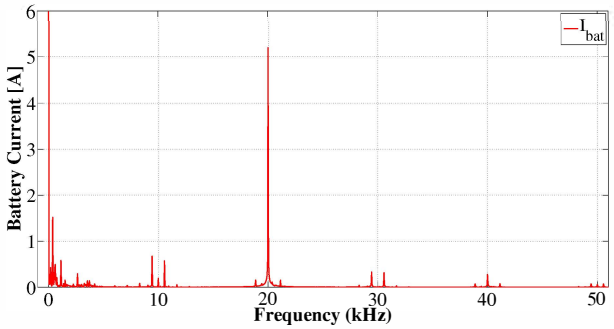

Fig. 14: Measurement: frequency spectrum of the battery current at 2262 rpm and 81 Nm.

The motor three-phase line currents are shown in Fig. 6 and the inverter dc side current is shown in Fig. 7. For an ideal system, the dc bus capacitor absorbs all of the high frequency components (non-dc) of the current, but for a realistic system there are some high frequency terms. The dc bus voltage is shown in Fig. 9. The value of the voltage is 343 V, and there is some ripple due to the switching in the system.

The battery current is depicted in Fig. 10; Fig. 8 shows the frequency spectrum of the battery current. The spectrum of the battery current shows that in addition to the dc component, there is a component around 3.6 kHz due to resonance between the cable and dc bus capacitor and some components around multiple of the carrier frequencies, i.e. 10 kHz, 20 kHz, and so on. The magnitude of the battery current harmonics for non-dc components is not high.

B. *Practical Verification*

To investigate different parts of the electrical system of a plug-in vehicle, extensive measurements have been performed, especially on the dc side of the traction circuit where a few results are presented here. Fig. 11 and 12 show the battery voltage and current at a speed of 2262 rpm and a torque level of 81 Nm. Moreover, the FFT of the battery voltage and current are show in Fig. 13 and 14. The plot is zoomed to magnify the harmonic components. So, the dc components

TABLE II: Measurement results for a single operation point in steady state.

	Value	Unit
Speed	2262	rpm
Torque	81	Nm
Peak phase current	190	A
Battery voltage	343	V
Battery current	60	A
i_d	-105	A
i_q	162	A
v_d	-75	V
v_q	34	V

is not fully shown in the figure.

As can bee seen from these figures, the practical results are very similar to the simulation values, as is expected from the theoretical formula. The major harmonics in the dc side are around the resonance frequency and multiples of carrier frequency due to PWM switching, i.e. 10 kHz and 20 kHz. Table II summarizes the measured values in steady state.

V. Conclusion

To investigate the quality of the dc bus of an electric or hybrid electric vehicle, the high-frequency model of the devices towards the dc terminals are needed. A harmonic model of the traction circuit based on a three-phase inverter and an ac motor towards the dc system is presented. The model is developed for a three-phase inverter with SPWM and a three-phase line current. For a vehicle traction system based on a FOC with a SPWM control strategy, the simulation results are provided and the results show an accurate agreement with the predicted frequency spectrum in the dc bus current and voltage. Measurements of a real vehicle are provided to verify the harmonic pattern in the dc bus, as is expected by using the equivalent circuit and simulation results. The main harmonics are around the resonance frequency of the dc bus capacitor and cable, and multiple of carrier frequency due to the PWM switching that is 10 kHz and 20 kHz.

References

[1] M. Anwar, S. Gleason, and T. Grewe, "Design considerations for high-voltage dc bus architecture and wire mechanization for hybrid and electric vehicle applications," in *Energy Conversion Congress and Exposition (ECCE), 2010 IEEE*, 2010, pp. 877–884.

[2] S. Haghbin, S. Lundmark, M. Alakula, and O. Carlson, "Grid-connected integrated battery chargers in vehicle applications: Review and new solution," *Industrial Electronics, IEEE Transactions on*, vol. 60, no. 2, pp. 459–473, 2013.

[3] A. Karvonen and T. Thiringer, "Simulating the emi characteristics of flyback dc/dc converters," in *Telecommunications Energy Conference (INTELEC), 2011 IEEE 33rd International*, 2011, pp. 1–7.

[4] M. Liukkonen, M. Hinkkanen, J. Kyyra, and S. Ovaska, "Modeling of multiport dc busses in power-electronic systems," in *Industrial Technology (ICIT), 2013 IEEE International Conference on*, 2013, pp. 740–745.

[5] S. Sudhoff, S. Glover, P. Lamm, D. H. Schmucker, and D. Delisle, "Admittance space stability analysis of power electronic systems," *Aerospace and Electronic Systems, IEEE Transactions on*, vol. 36, no. 3, pp. 965–973, 2000.

[6] J. Liu, X. Feng, F. Lee, and D. Borojevich, "Stability margin monitoring for dc distributed power systems via perturbation approaches," *Power Electronics, IEEE Transactions on*, vol. 18, no. 6, pp. 1254–1261, 2003.

[7] Z. Peroutka, "Motor insulation breakdowns due to operation of frequency converters," in *Power Tech Conference Proceedings, 2003 IEEE Bologna*, vol. 2, 2003, pp. 8 pp. Vol.2–.

[8] A. Khaligh, A. Rahimi, and A. Emadi, "Negative impedance stabilizing pulse adjustment control technique for dc/dc converters operating in discontinuous conduction mode and driving constant power loads," *Vehicular Technology, IEEE Transactions on*, vol. 56, no. 4, pp. 2005–2016, 2007.

[9] S. Haghbin and T. Thirniger, *High-Frequency Modeling of a Three-Phase Inverter with Sinusoidal Pulse Width Modulation Control*. Chalmers University of Technology, Internal report, 2014.

[10] S. Haghbin, *An Isolated Integrated Charger for Electric or Plug-in Hybrid Vehicles*. Licentiate Thesis, Chalmers University of Technology, 2011.

[11] D. Vindel, S. Haghbin, A. Rabiei, O. Carlson, and R. Ghorbani, "Field-oriented control of a pmsm drive system using the dspace controller," in *Electric Vehicle Conference (IEVC), 2012 IEEE International*, 2012, pp. 1–5.

[12] M. Haque and M. Rahman, "Control trajectories for interior permanent magnet synchronous motor drives," in *Electric Machines Drives Conference, 2007. IEMDC '07. IEEE International*, vol. 1, may 2007, pp. 306 –311.

[13] S. Haghbin, *Integrated Motor Drives and Battery Chargers for Electric or Plug-in Hybrid Electric Vehicles*. PhD Thesis, Chalmers University of Technology, 2013.

[14] F. Savoye, P. Venet, M. Millet, and J. Groot, "Impact of periodic current pulses on li-ion battery performance," *Industrial Electronics, IEEE Transactions on*, vol. 59, no. 9, pp. 3481–3488, Sept 2012.

[15] P. Dahono, A. Purwadi, and T. Kataoka, "A new approach for harmonic analysis of three-phase current-type pwm converters," in *Industry Applications Conference, 1997. Thirty-Second IAS Annual Meeting, IAS '97., Conference Record of the 1997 IEEE*, vol. 2, 1997, pp. 1487–1495 vol.2.